

**Measurement of the fusion probability,  $P_{\text{CN}}$ , for hot fusion reactions**

R. Yanez, W. Loveland, J. S. Barrett, and L. Yao

*Department of Chemistry, Oregon State University, Corvallis, Oregon 97331, USA*

B. B. Back, S. Zhu, and T. L. Khoo

*Physics Division, Argonne National Laboratory, Argonne, Illinois 60439, USA*

(Received 30 May 2013; published 17 July 2013)

**Background:** The cross section for forming a heavy evaporation residue in fusion reactions depends on the capture cross section, the fusion probability,  $P_{\text{CN}}$ , i.e., the probability that the projectile-target system will evolve inside the fission saddle point to form a completely fused system rather than reseparating (quasifission), and the survival of the completely fused system against fission.  $P_{\text{CN}}$  is the least known of these quantities.

**Purpose:** We want to determine  $P_{\text{CN}}$  for the reactions of 101.2 MeV  $^{18}\text{O}$ , 147.3 MeV  $^{26}\text{Mg}$ , 170.9 MeV  $^{30}\text{Si}$ , and 195.3 MeV  $^{36}\text{S}$  with  $^{197}\text{Au}$ .

**Methods:** We measured the fission fragment angular distributions for these reactions and used the formalism of Back to deduce the fusion-fission and quasifission cross sections. From these quantities we deduced  $P_{\text{CN}}$  for each reaction.

**Results:** The values of  $P_{\text{CN}}$  for the reactions of 101.2 MeV  $^{18}\text{O}$ , 147.3 MeV  $^{26}\text{Mg}$ , 170.9 MeV  $^{30}\text{Si}$ , and 195.3 MeV  $^{36}\text{S}$  with  $^{197}\text{Au}$  are 0.66, 1.00, 0.06, and 0.13, respectively.

**Conclusions:** The new measured values of  $P_{\text{CN}}$  agree roughly with the semiempirical systematic dependence of  $P_{\text{CN}}$  upon fissility for excited nuclei.

DOI: [10.1103/PhysRevC.88.014606](https://doi.org/10.1103/PhysRevC.88.014606)

PACS number(s): 25.70.Jj, 25.85.-w, 25.60.Pj

**I. INTRODUCTION****A. Motivation**

The remarkable recent progress in the synthesis of new heavy and superheavy nuclei has been made using fusion reactions. These reactions can be divided into two prototypical classes, “cold” and “hot” fusion reactions. In cold fusion reactions, one bombards Pb or Bi target nuclei with heavier projectiles (Ca–Kr) to form completely fused systems with low excitation energies ( $E^* = 10\text{--}15$  MeV), leading to a higher survival (against fission) but with a reduced probability of the fusion reaction taking place due to the larger Coulomb repulsion in the more symmetric reacting system. (This approach has been used in the synthesis of elements 107–113). In hot fusion reactions one uses a more asymmetric reaction (typically involving a lighter projectile and an actinide target nucleus) to increase the fusion probability but leading to a highly excited completely fused system ( $E^* = 30\text{--}60$  MeV) with a reduced probability of surviving against fission. (This approach has been used to synthesize elements 102–118.)

Formally, the cross section for producing a heavy evaporation residue,  $\sigma_{\text{EVR}}$ , in a fusion reaction can be written as

$$\sigma_{\text{EVR}} = \sum_{J=0}^{J_{\text{max}}} \sigma_{\text{capture}}(E_{\text{c.m.}}, J) P_{\text{CN}}(E^*, J) W_{\text{sur}}(E^*, J), \quad (1)$$

where  $\sigma_{\text{capture}}(E_{\text{c.m.}}, J)$  is the capture cross section at center-of-mass energy  $E_{\text{c.m.}}$  and spin  $J$ .  $P_{\text{CN}}$  is the probability that the projectile-target system will evolve from the contact configuration inside the fission saddle point to form a completely fused system rather than reseparating (quasifission, fast fission).  $W_{\text{sur}}$  is the probability that the completely fused

system will deexcite by neutron emission rather than fission. For a quantitative understanding of the synthesis of new heavy nuclei, one needs to understand  $\sigma_{\text{capture}}$ ,  $P_{\text{CN}}$ , and  $W_{\text{sur}}$  for the reaction system under study.

The capture cross section is, in the language of coupled channel calculations, the “barrier crossing” cross section. It is the sum of the quasifission, fast fission, fusion-fission, and fusion-evaporation residue cross sections. The latter cross section is so small for the systems studied in this work that it is neglected. In these hot fusion reactions, the capture cross sections have either been measured [1–4] or can be predicted, with reasonable accuracy by semiempirical systematics [5] or more fundamental calculations [6,7]. From a knowledge of  $\sigma_{\text{EVR}}$  and  $\sigma_{\text{capture}}$ , one can calculate the value of the product  $W_{\text{sur}} P_{\text{CN}}$ .

The survival probabilities,  $W_{\text{sur}}$ , are calculated using well established formalisms [8,9] where the principal uncertainty is the value of the fission barrier height. Calculations of hot fusion reactions are particularly susceptible to this uncertainty due to the occurrence of multiple chance fission. (The best recent calculations [10] of superheavy element fission barrier heights indicate an average discrepancy between data and theory of about 0.4 MeV with the largest discrepancy being about 1.0 MeV. This latter number roughly translates into an order-of-magnitude uncertainty in the fission rate). Nonetheless, the operational procedures for calculating  $W_{\text{sur}}$  are fairly well understood as well as the dependence of  $W_{\text{sur}}$  on reaction parameters.

The fusion probability,  $P_{\text{CN}}$ , is the least well known quantity that determines the evaporation residue cross section [11]. Not only is the numerical value of  $P_{\text{CN}}$  uncertain, but the dependence of  $P_{\text{CN}}$  on excitation energy [11–13] and the reaction entrance channel is not well established [13]. It is this quantity,  $P_{\text{CN}}$ , that is the focus of this work.

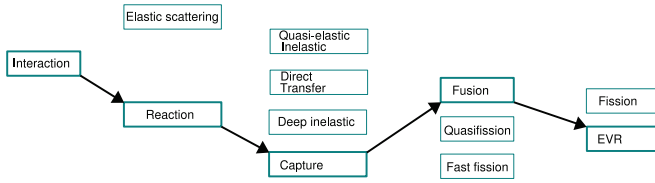


FIG. 1. (Color online) Schematic diagram of the path to synthesize new heavy nuclei, showing the reaction mechanisms involved.

## B. Reaction mechanisms

When a projectile nucleus interacts or reacts with a heavy target nucleus, there are several possible outcomes and/or mechanisms that come into play (Fig. 1). The process of bringing the reacting nuclei into contact and surmounting the interaction barrier is referred to as “capture” whose probability is reflected in  $\sigma_{\text{capture}}$ . Capture can lead to several different outcomes and/or mechanisms, i.e., fusion, quasifission, and fast fission. We briefly summarize the characteristics of each of these dissipative processes as follows: [14,15].

**Fusion.** After full momentum transfer, the reacting system evolves inside the fission saddle point, resulting in long interaction times and either formation of evaporation residues (fusion-evaporation) (products of complete fusion that deexcite by particle emission) or the formation of mass symmetric fission fragments (fusion-fission).

**Quasifission.** After full momentum transfer, and intermediate interaction times, the reacting system *does not* evolve inside the fission saddle point, but reseparates either without significant mass exchange (asymmetric quasifission) or with significant mass transfer (symmetric quasifission). In any case the fragment angular distributions are more anisotropic than those resulting from fusion-fission.

**Fast fission.** After full momentum transfer and mass drift, the resulting mononucleus fissions because there is no fission barrier, due to the large angular momentum,  $J$ , of the system. Fast fission is not relevant for situations where  $J$  is less than the rotating liquid drop limit. Although fast fission is mechanistically different from quasifission (involving a different range of angular momenta), it is not possible experimentally to distinguish fast fission and quasifission. They are both nonfusing collisions. In many discussions, fast fission is included in the quasifission component. To complicate matters, in the older literature, the term “fast fission” was frequently used to refer to what we now call quasifission.

The capture cross section,  $\sigma_{\text{capture}}$ , is thus

$$\sigma_{\text{capture}} = \sigma_{\text{fusion}} + \sigma_{\text{quasifission}} + \sigma_{\text{fast fission}}, \quad (2)$$

while  $\sigma_{\text{fusion}}$ , the fusion cross section, is

$$\sigma_{\text{fusion}} = \sigma_{\text{fusion-evaporation}} + \sigma_{\text{fusion-fission}}, \quad (3)$$

where  $\sigma_{\text{quasifission}}$  is the quasifission cross section and  $\sigma_{\text{fast fission}}$  is the fast fission cross section.  $P_{\text{CN}}$  is defined as

$$P_{\text{CN}} = \frac{\sigma_{\text{fusion}}}{\sigma_{\text{capture}}} = \frac{\sigma_{\text{capture}} - \sigma_{\text{quasifission}} - \sigma_{\text{fast fission}}}{\sigma_{\text{capture}}} \quad (4)$$

## C. Quasifission

The measurement of  $P_{\text{CN}}$  requires the identification and separation of fusion, quasifission, and fast fission (where relevant). Primarily this task becomes one of identifying quasifission, the reseparation of the contacting nuclei before moving inside the fission saddle point. There are a series of natural questions about quasifission that are relevant for this problem. When does quasifission occur? What are its measurable characteristics? What are the relevant theoretical models and predictions about quasifission? What are the experimental data about quasifission?

When does quasifission occur? Three general, semiempirical answers to this question are (a) when the mean fissility of the reacting system,  $x_m$ , exceeds 0.72 [16,17]; (b) when the product of the atomic numbers of the reacting nuclei,  $Z_1 Z_2$ , exceeds 1600 [1,16,18–21]; and (c) when the asymmetry,  $\alpha$ , of the reacting system is less than the mass asymmetry associated with the Businaro-Gallone point [22–26]. Unfortunately there are known exceptions to each of these general rules, i.e., (a) [24,27,28], (b) [29–31], and (c) [31,32].

What are the measurable characteristics of quasifission? Historically quasifission has been identified by a broadening of the fragment mass distributions caused by the presence of asymmetric mass distributions due to quasifission [14,26,33] and by anomalously large fragment anisotropies relative to those expected from fusion-fission [34,35].

Initially one associated symmetric fission with fusion-fission, but it was realized that quasifission could lead to mass symmetric fission fragments [36,37]. One also realized the utility of looking at the correlation between fission fragment masses and their angular distributions [20,21,38].

What are the relevant theoretical models and predictions about quasifission? Zagrebaev and Greiner have done a number of calculations of  $P_{\text{CN}}$  using various approaches [39,40], culminating in some simple semiempirical predictions for  $P_{\text{CN}}(E^*)$  and  $P_{\text{CN}}(Z, A)$  for cold fusion reactions [11]. There have been a number of calculations of  $P_{\text{CN}}$  using the dinuclear system (DNS) approach for both hot and cold fusion reactions [12,15,41–43] that differ from the Zagrebaev and Greiner predictions [11]. A number of calculations of  $P_{\text{CN}}$  for cold fusion reactions have been made using the “fusion by diffusion” approach [5,44–46] that differs from both the DNS and Zagrebaev and Greiner approaches. There have also been a number of attempts [25,44,46,47] to make semiempirical estimates of  $P_{\text{CN}}$  using one or another models for  $\sigma_{\text{capture}}$  and  $W_{\text{sur}}$ , and using measured values for  $\sigma_{\text{EVR}}$  to get values of  $P_{\text{CN}}$  for both hot and cold fusion reactions. Other aspects of quasifission, such as the time scale and the role of deformation effects in the entrance channel, have been treated [38,48–50]. Contradictory results have been obtained both experimentally [13] and theoretically [11,12] for the expected dependence of  $P_{\text{CN}}$  upon excitation energy.

What are the experimental data about quasifission and  $P_{\text{CN}}$ ? In Table I, we attempt to list the current measurements of  $P_{\text{CN}}$ . The data are sorted by the values of  $Z_1 Z_2$ , which serves as an approximate scaling variable, although values of  $P_{\text{CN}} \leq 1$  are observed for values of  $Z_1 Z_2 \leq 1600$ . The data described in Table I, of necessity, do not include cases

TABLE I. Measurements of  $P_{CN}$ . The methods are angular distribution measurements (AD), mass distribution measurements (MY), and mass-angle measurements (MAD).

Proj.	Target	CN	$E_{c.m.}$ (MeV)	$E^*$ (MeV)	$Z_1 Z_2$	$\alpha$	$\alpha_{BG}$	$x_{eff}$	$P_{CN}$	Ref.	Method
$^{11}\text{B}$	$^{204}\text{Pb}$	$^{215}\text{At}$	48–60	31–43	410	0.898	0.761	0.325	1–1	[32]	AD
$^{16}\text{O}$	$^{186}\text{W}$	$^{202}\text{Pb}$	70–121	48–100	592	0.842	0.765	0.42	1–1	[31]	MAD
$^{18}\text{O}$	$^{197}\text{Au}$	$^{215}\text{At}$	71–89	39–56	632	0.833	0.788	0.413	1–1	[32]	AD
$^{19}\text{F}$	$^{208}\text{Pb}$	$^{227}\text{Pa}$	101–174	51–124	738	0.833	0.816	0.459	0.78–0.83	[34]	AD
$^{24}\text{Mg}$	$^{208}\text{Pb}$	$^{232}\text{Pu}$	126–188	52–114	984	0.793	0.847	0.549	0.64–0.71	[34]	AD
$^{48}\text{Ca}$	$^{144}\text{Sm}$	$^{192}\text{W}$	141–167	38–64	1080	0.5	0.756	0.544	1–1	[31]	MAD
$^{28}\text{Si}$	$^{208}\text{Pb}$	$^{236}\text{Cm}$	141–229	50–138	1148	0.763	0.862	0.597	0.37–0.63	[34]	AD
$^{26}\text{Mg}$	$^{248}\text{Cm}$	$^{274}\text{Hs}$	119–146	37–64	1152	0.81	0.886	0.572	0.6	[68]	MY
$^{32}\text{S}$	$^{182}\text{W}$	$^{214}\text{Th}$	141–221	56–136	1184	0.701	0.851	0.613	0.14–0.51	[62]	AD
$^{48}\text{Ca}$	$^{154}\text{Sm}$	$^{202}\text{Pb}$	139–185	49–95	1240	0.525	0.813	0.594	0.55–0.94	[31]	MAD
$^{40}\text{Ca}$	$^{154}\text{Sm}$	$^{194}\text{Pb}$	139–158	56–75	1240	0.588	0.828	0.633	0.89–0.98	[31]	MAD
$^{32}\text{S}$	$^{208}\text{Pb}$	$^{240}\text{Cf}$	172–217	66–111	1312	0.733	0.875	0.641	0.45–0.46	[34]	AD
$^{36}\text{S}$	$^{238}\text{U}$	$^{274}\text{Hs}$	153–173	36–56	1472	0.737	0.896	0.647	0.043–0.3	[68]	MY
$^{50}\text{Ti}$	$^{208}\text{Pb}$	$^{258}\text{Rf}$	184–202	14–33	1804	0.612	0.899	0.725	0.02–0.19	[13]	AD
$^{48}\text{Ca}$	$^{238}\text{U}$	$^{286}\text{Cn}$	185–215	26–56	1840	0.664	0.911	0.713	0.00025–0.125	[69]	MY
$^{64}\text{Ni}$	$^{238}\text{U}$	$^{302}\text{120}$	267–300	30–63	2576	0.576	0.939	0.867	0.021–0.047	[69]	MY

where  $P_{CN} \ll 1$  because the complete fusion fraction is not measurable, generally, for  $P_{CN} \leq 0.01$ . If one restricts oneself to  $E^* \sim 40$ – $50$  MeV (to remove the dependence of  $P_{CN}$  upon  $E^*$ ), one can discern a rough empirical dependence of  $P_{CN}$  upon fissility (Fig. 2). The data near  $x_{eff} \sim 0.6$  involve  $^{48}\text{Ca}$  projectiles, perhaps reflecting the effects of nuclear structure in the entrance channel upon fusion probability [51,52]. To verify these apparent trends and to allow possible extrapolation and/or interpolation of these data, there is a need for a single measurement of  $P_{CN}$  that spans a large range in entrance channel asymmetry at a meaningful excitation energy.

#### D. This paper

In this report, we describe an experimental study that attempts to directly measure  $P_{CN}$  in a series of hot fusion reactions and thus to help resolve the fissility dependence of

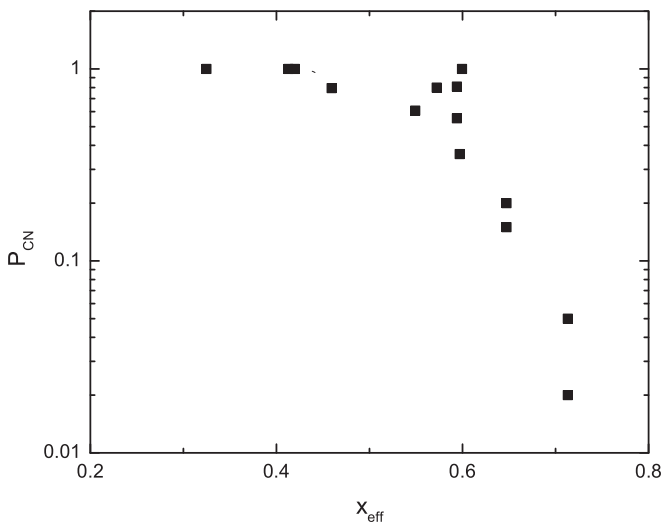


FIG. 2. A plot of measured values of  $P_{CN}$  vs the scaling parameter, the effective fissility,  $x_{eff}$ . The data are from Table I for systems where  $E^* \sim 40$ – $50$  MeV.

$P_{CN}$ . Specifically we measured the fission cross section and fragment angular distributions for the reactions of 101.2 MeV  $^{18}\text{O}$ , 147.3 MeV  $^{26}\text{Mg}$ , 170.9 MeV  $^{30}\text{Si}$ , and 195.3 MeV  $^{36}\text{S}$  with  $^{197}\text{Au}$ . These systems are described in Table II where we show that each system has an excitation energy  $E^*$  of about 60 MeV. The systems span a range in fissility similar to that covered in the data in Fig. 2. From these data, we have used the method of Back [34] to deduce the quasifission and complete fusion-fission components of the fragment angular distributions. We believe (see below) that this method is the best current method of measuring  $P_{CN}$ . (We have used this method previously in a study of  $P_{CN}$  in cold fusion reactions [13].) The values of  $P_{CN}$  are then compared with current predictions of these quantities.

Some of the systems studied in this work have been studied previously, i.e., the reaction of  $^{18}\text{O}$  with  $^{197}\text{Au}$  [25,32,53]. In [32], the fragment angular distributions were measured for the reaction of 78–97 MeV  $^{18}\text{O}$  with  $^{197}\text{Au}$ . The angular distributions were shown to be consistent with the standard theory of fragment angular distributions, thus indicating that  $P_{CN}$  is 1. This system can thus be a check on the reproducibility of the experimental measurements and their interpretation. Corradi *et al.*, [53] measured the yields of the Fr evaporation residues from the  $^{18}\text{O} + ^{197}\text{Au}$  reaction for beam energies of 75–130 MeV. Sagaidak *et al.* [25] took these data on evaporation residue production cross sections and compared them to the predictions of the computer code HIVAP assuming  $P_{CN}$  was 1. For a best fit to the data, they had to assume a reduction in the fission barrier height of 15%, which could also, as the authors point out, be taken as a need to decrease  $P_{CN}$ . Another related study [54] was that of the fragment angular distributions in the reaction of 185 MeV  $^{32}\text{S}$  with  $^{197}\text{Au}$ , where larger fragment anisotropies were observed than predicted by a rotating liquid model of the fissioning nucleus and the excitation energy  $E^*$  was 60 MeV. The fragment angular distributions were measured radiochemically for the interaction of  $^{11}\text{B}$ ,  $^{12}\text{C}$ ,  $^{14}\text{N}$ , and  $^{16}\text{O}$ , with  $^{197}\text{Au}$  [55]. The data are well described by the standard theory of fission

TABLE II. Characteristics of reactions studied in this work.

Proj.	Target	CN	$E_{c.m.}$ (MeV)	$E^*$ (MeV)	$Z_1 Z_2$	$\alpha$	$\alpha_{BG}$	$x_{eff}$	$\sigma_{capture-fission}$ (mb)	$P_{CN}$
$^{18}\text{O}$	$^{197}\text{Au}$	$^{215}\text{At}$	92.8	60.5	632	0.833	0.788	0.413	$834 \pm 4$	0.66
$^{26}\text{Mg}$	$^{197}\text{Au}$	$^{223}\text{Pa}$	130.1	60.4	948	0.767	0.833	0.524	$749 \pm 6$	1.0
$^{30}\text{Si}$	$^{197}\text{Au}$	$^{227}\text{Np}$	148.3	60.2	1106	0.736	0.849	0.572	$770 \pm 10$	0.06
$^{36}\text{S}$	$^{197}\text{Au}$	$^{233}\text{Am}$	165.1	60.1	1264	0.691	0.860	0.604	$748 \pm 10$	0.13

fragment angular distributions [8], except that there were some difficulties due to the occurrence of incomplete fusion at higher bombarding energies, and the extracted values of the mean spin of the fissioning systems were low for reactions near the Coulomb barrier.

In summary, previous work supports the idea that  $P_{CN}$  is 1 for the most asymmetric systems involving the interaction of lighter projectiles with  $^{197}\text{Au}$ .

## II. EXPERIMENTAL METHODS

The experiment was carried out in the ATSCAT scattering chamber at the ATLAS accelerator facility at the Argonne National Laboratory. The experimental setup is shown in Fig. 3. Beams of  $^{18}\text{O}$ ,  $^{26}\text{Mg}$ ,  $^{30}\text{Si}$ , and  $^{36}\text{S}$  struck a  $^{197}\text{Au}$  target mounted at the center of the scattering chamber. We assumed that all ion charges equilibrated in the  $0.25 \text{ mg/cm}^2$   $^{197}\text{Au}$  target and the equilibrium charge values [56] were used in calculating beam doses. The beam intensity was monitored in two ways: (a) by a deep Faraday cup at the periphery of the chamber and (b) by a pair of silicon monitor detectors ( $r = 2.00 \text{ mm}$ ) mounted at  $15^\circ$  with respect to the beam axis at a distance of  $412.75 \text{ mm}$  from the target. A voltage of  $+9 \text{ kV}$  was applied to the target to suppress the emission of energetic  $\delta$  electrons. The beam intensities ranged from  $2$  to  $3 \times 10^{10} \text{ p/s}$ . All beam energies used herein are the center of target beam energies calculated using SRIM [57].

On one side of the beam, we mounted an array of Si detectors whose positions were fixed during all measurements. The angles of these detectors were  $73^\circ$ ,  $78^\circ$ ,  $83^\circ$ , and  $89^\circ$ . On the other side of the beam there were two independently movable arrays, one at forward angles and one at backward angles. The forward array consisted of three detectors nominally separated in angle by  $5^\circ$ . The backward array

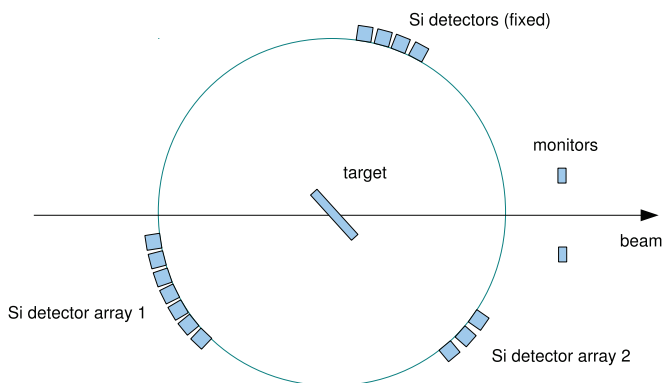


FIG. 3. (Color online) Schematic diagram of the experimental apparatus.

consisted of seven detectors nominally separated by  $5^\circ$  from each other. All the array detectors had an area of  $300 \text{ mm}^2$  and were positioned at  $\sim 320 \text{ mm}$  from the target. For each projectile-target combination, six positions of the forward and backward arrays were used. For the backward array angles of  $82^\circ$ – $172^\circ$  were sampled while the forward array was used for measurements at angles of  $53^\circ$ – $75^\circ$ .

Time information was measured for each Si detector relative to the Linac pulse structure. The beam was bunched into packets with a FWHM of  $0.71 \text{ ns}$ . The average time between beam bursts was  $82 \text{ ns}$ . From the particle time of flight and energy, the mass of the fragment was calculated.

Energy calibrations of each Si detector were performed using the response of the detectors to  $^{252}\text{Cf}$  fission fragments and elastically scattered beam from a  $^{197}\text{Au}$  target. A correction for pulse height defect was applied to fission fragments striking the detectors, using the response of the detectors to  $^{252}\text{Cf}$  fission fragments [58].

The reaction of heavy ions with  $^{197}\text{Au}$  can lead to elastic scattering, inelastic scattering, deep inelastic scattering, fusion-fission, quasifission, and fusion-evaporation residue formation. (The cross section for evaporation residue formation is small in comparison with the other processes and will be neglected in this discussion). Fusion-fission and quasifission events were isolated from the other types of events by analyzing the  $E$ -vs- $A$  response of each detector.

## III. RESULTS

### A. Capture cross sections

The singles fission data at backward angles was integrated using data with  $\theta_{lab} \leq 172^\circ$ . The total cross section was deduced from these differential cross sections by the simple assumption that the fission fragments were emitted in a plane perpendicular to the total angular momentum vector; i.e., the fragment angular distribution is given by

$$W(\theta) = (2\pi^2 \sin \theta)^{-1}. \quad (5)$$

The resulting capture-fission cross sections are shown in Fig. 4 and Table II. In Fig. 4, we also show a previous measurement of  $\sigma_{capture-fission}$  for the reaction of  $97 \text{ MeV } ^{18}\text{O} + ^{197}\text{Au}$  [32]. We also show a measurement of  $\sigma_{capture-fission}$  for the reaction of  $185 \text{ MeV } ^{32}\text{S} + ^{197}\text{Au}$  [54] where the measured cross section of  $250 \pm 15 \text{ mb}$  has been scaled (multiplied by) the ratio of the Bass model fusion cross sections (1.55) for the  $185 \text{ MeV } ^{32}\text{S} + ^{197}\text{Au}$  and the  $195.3 \text{ MeV } ^{36}\text{S} + ^{197}\text{Au}$  cross sections. We also show the predictions for these cross sections obtained using two statistical model codes for heavy element reactions, HIVAP [59] and the coupled channels approach of

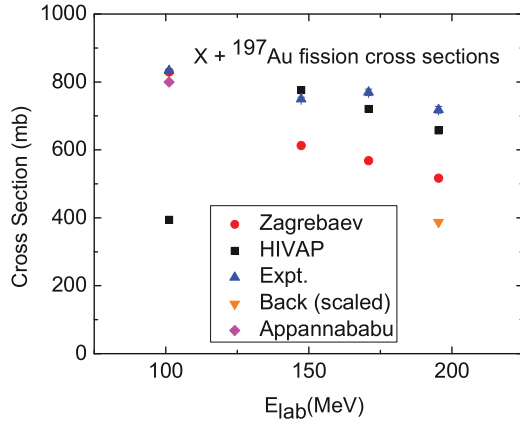


FIG. 4. (Color online) Measured capture-fission cross sections for the reactions studied in this work along with previous measurements [32,54] and statistical model estimates of these cross sections [9,59]. The laboratory energies for the  $^{18}\text{O}$ ,  $^{26}\text{Mg}$ ,  $^{30}\text{Si}$ , and  $^{36}\text{S}$  reactions were 101.2, 147.3, 170.9, and 195.3 MeV, respectively.

Zagrebaev [9]. The discordance amongst the measurements and the predictions is discouraging although this situation is consistent with previous evaluations of factors of 2–10 discrepancies in calculating  $\sigma_{\text{capture}}$  [60,61].

### B. Fragment angular distributions

The fission fragment angular distributions were measured using the individual Si detectors and are shown in Fig. 5.

It has been shown [34,62] that for some reactions a significant fraction of the fission events result from “quasifission” as well as “true complete fusion.” Quasifission is the process where the interacting nuclei merge to form a mononucleus

but the system does not evolve inside the fission saddle point. For the purpose of estimating heavy element production by complete fusion, one must separate the contributions of quasifission and true complete fusion in the data. Using the methods outlined in Refs. [34,62], which depend on analyzing the shape of the fission fragment angular distributions, we have attempted to estimate the relative contributions of quasifission and complete fusion to the observed cross sections.

The authors of [34,62] studied the angular distributions for a large number of reactions. They concluded that one could decompose the observed fission angular distributions into two components, one due to complete fusion and the other due to quasifission. The complete fusion component has an angular distribution characterized by values of the effective moment of inertia,  $\mathfrak{S}_{\text{eff}}$ , as taken from the rotating liquid drop model [63,64] for  $J \leq J_{\text{CN}}$ , while the quasifission component has

$$\frac{\mathfrak{S}_0}{\mathfrak{S}_{\text{eff}}} = 1.5 \quad \text{for } J > J_{\text{CN}}. \quad (6)$$

Figure 12 in [65] shows the shapes associated with various values of  $\mathfrak{S}_0/\mathfrak{S}_{\text{eff}}$ .

In these equations,  $\mathfrak{S}_0$  is the moment of inertia of a spherical nucleus with the same  $A$  value, complete fusion is assumed to occur for spins  $0 \leq J \leq J_{\text{CN}}$  and quasifission is assumed to occur for spins  $J > J_{\text{CN}}$ . We fitted the observed fission fragment angular distributions allowing the maximum angular momentum associated with complete fusion,  $J_{\text{CN}}$ , to be a free parameter determined in the calculation. ( $J_{\text{max}}$  was determined from the sum of the complete fusion-fission and quasifission cross sections using a sharp cutoff approximation. In the  $^{36}\text{S} + ^{197}\text{Au}$  reaction,  $J_{\text{max}}$  was restricted to be  $64\hbar$ , the rotating liquid drop limit [64].) We used the familiar expressions for the fission fragment angular distributions [66],

$$W(\theta) = \sum_{J=0}^{J_{\text{CN}}} \frac{(2J+1)^2 \exp[-(J+1/2)^2 \sin^2 \theta / 4K_0^2(F)] J_0[i(J+1/2)^2 \sin^2 \theta / 4K_0^2(F)]}{\text{erf}[(J+1/2)/(2K_0^2(F))^{1/2}]} + \sum_{J=J_{\text{CN}}}^{J_{\text{max}}} \frac{(2J+1)^2 \exp[-(J+1/2)^2 \sin^2 \theta / 4K_0^2(Q)] J_0[i(J+1/2)^2 \sin^2 \theta / 4K_0^2(Q)]}{\text{erf}[(J+1/2)/(2K_0^2(Q))^{1/2}]}, \quad (7)$$

neglecting the spins of the target and projectile, where  $J_0$  is the zero-order Bessel function with imaginary argument and the error function  $\text{erf}[(J+1/2)/(2K_0^2)^{1/2}]$  is defined as

$$\text{erf}(x) = (2/\pi^{1/2}) \int_0^x \exp(-t^2) dt. \quad (8)$$

The parameter  $K_0^2$  is defined as

$$K_0^2 = T \mathfrak{S}_{\text{eff}} / \hbar^2, \quad (9)$$

$$\frac{1}{\mathfrak{S}_{\text{eff}}} = \frac{1}{\mathfrak{S}_{\parallel}} - \frac{1}{\mathfrak{S}_{\perp}}, \quad (10)$$

where the nuclear temperature at the saddle point  $T$  is given as

$$T = \left[ \frac{E^* - B_f - E_{\text{rot}} - E_v}{A/8.5} \right]^{1/2} \quad (11)$$

and  $\mathfrak{S}_{\parallel}$  and  $\mathfrak{S}_{\perp}$  are the moments of inertia for rotations around the axes parallel and perpendicular to the nuclear symmetry axis, respectively.  $B_f$ ,  $E_{\text{rot}}$ , and  $E_v$  are the fission barrier, the rotational energy of the system, and the energy lost in the emission of pre-fission neutrons. This later quantity is taken from estimates from [9]. The assumption that

$$\frac{\mathfrak{S}_0}{\mathfrak{S}_{\text{eff}}} = 1.5 \quad \text{for } J > J_{\text{CN}}, \quad (12)$$

for quasifission is arbitrary. This assumed value of the ratio  $\frac{\mathfrak{S}_0}{\mathfrak{S}_{\text{eff}}}$  is greater than that observed in any complete fusion-fission reaction [34], but the actual value of this ratio is not well established.

In fitting the angular distribution data, one uses the measured value of  $\sigma_{\text{capture}}$ , and  $K_0^2$  values calculated from

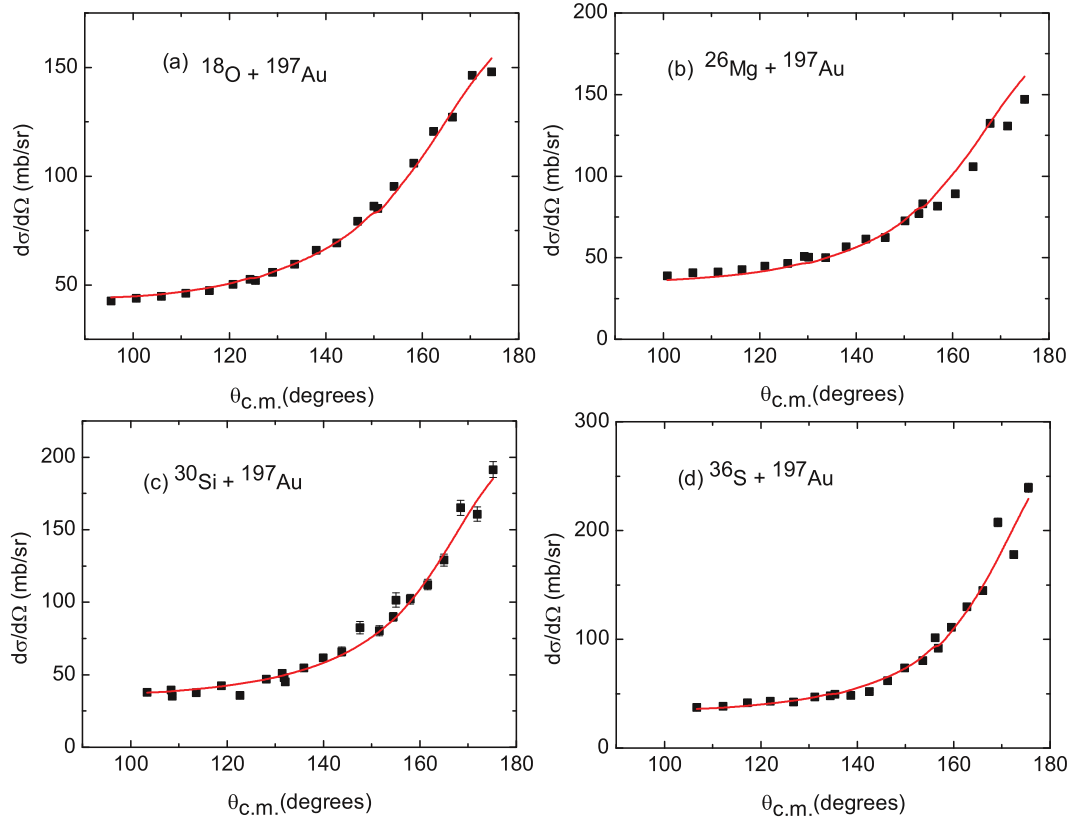


FIG. 5. (Color online) Measured fission fragment angular distributions for the reactions studied in this work and the resulting fits to the distributions to resolve complete fusion-fission from quasifission.

Eq. (9) and varies  $J_{\text{CN}}$  until a minimum in the reduced chi-square value,  $\chi_v^2$ , is achieved. Then

$$\frac{J_{\text{CN}}^2}{J_{\text{max}}^2} = \frac{\sigma_{\text{CN}}}{\sigma_{\text{capture}}} = P_{\text{CN}}. \quad (13)$$

The final fits to the measured angular distributions are shown in Fig. 5. The deduced values of  $P_{\text{CN}}$  for the reactions of 101.2 MeV  $^{18}\text{O}$ , 147.3 MeV  $^{26}\text{Mg}$ , 170.9 MeV  $^{30}\text{Si}$ , and 195.3 MeV  $^{36}\text{S}$  with  $^{197}\text{Au}$  are 0.66, 1.00, 0.06, and 0.13, respectively. For all cases, the  $\chi_v^2$  values were statistically significant at the 95 % level [67]. It is difficult to make meaningful estimates of the uncertainties in the deduced values of  $P_{\text{CN}}$  given the fundamental systematic uncertainties in  $\frac{\mathcal{J}_0}{\mathcal{J}_{\text{eff}}}$  and thus in  $K_0^2$ .

#### IV. DISCUSSION

From analyzing our data for the reaction of 101.2 MeV  $^{18}\text{O}$  with  $^{197}\text{Au}$ , we deduced a value of  $P_{\text{CN}}$  of 0.66. The authors of [32] found their angular distributions for the reaction of 97 MeV  $^{18}\text{O}$  with  $^{197}\text{Au}$  were consistent with the standard theory of angular distributions, presumably indicating  $P_{\text{CN}} = 1$ . Sagaidak *et al.* [25] analyzed the evaporation residue data of Corradi *et al.* [53] for 75–130 MeV  $^{18}\text{O} + ^{197}\text{Au}$  and found the fission barriers had to be lowered by a factor of 0.75 to fit the data. They noted a similar situation in the  $^{19}\text{F} + ^{197}\text{Au}$  reaction where the similar results (scaling

factor = 0.85) could also be accounted for if  $P_{\text{CN}} = 0.75$ . Another relevant observation is that of Viola, Thomas, and Seaborg [55], who studied the fragment angular distributions in the closely related  $^{16}\text{O} + ^{197}\text{Au}$  reaction and who found they were unable to describe the distributions with standard methods. Given all this information, our measured value of  $P_{\text{CN}} = 0.66$  for the reaction of 101.2 MeV  $^{18}\text{O}$  with  $^{197}\text{Au}$  seems reasonable.

Back *et al.* [54] have previously measured and analyzed the fission fragment angular distributions for the reaction of 185–225 MeV  $^{32}\text{S} + ^{197}\text{Au}$ . They concluded that the value of  $\frac{\mathcal{J}_0}{\mathcal{J}_{\text{eff}}}$  needed to describe the data was significantly different (1.5–2 times) from that predicted by the rotating liquid drop model. That is qualitatively consistent with our finding of  $P_{\text{CN}} = 0.13$  for the  $^{36}\text{S} + ^{197}\text{Au}$  system.

In Fig. 6, we compare our measured values of  $P_{\text{CN}}$  (from this work) to the systematics of  $P_{\text{CN}}$  values [60] for systems with  $E^* = 40$ –50 MeV. (Strictly speaking, since all the systems studied in this work involve  $E^* \sim 60$  MeV, we should scale the measured values to  $E^* = 40$ –50 MeV. However, because of the controversy [11,12] about how to do this scaling, we are just plotting our unscaled data.)

All the new data values of  $P_{\text{CN}}$  are within an order of magnitude of the systematic trend of the previous data. (That is consistent with general predictions of the uncertainties in our knowledge of  $P_{\text{CN}}$  [61].) Zagrebaev and Greiner have suggested [11] that, for data where  $E^* \leq 40$  MeV, that  $P_{\text{CN}}$  (at

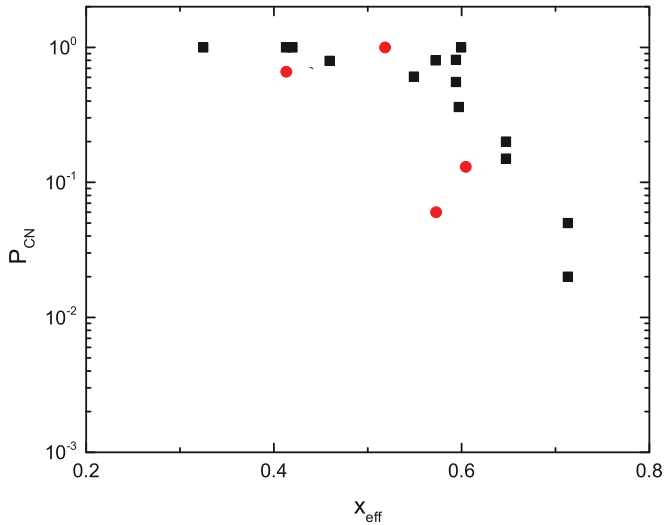


FIG. 6. (Color online) Comparison of the measurements from this work with the systematic dependence of  $P_{\text{CN}}$  upon fissility. The red circles are the data from this work while the black squares represent previous measurements.

constant  $E^*$ ) might show a simple behavior,

$$P_{\text{CN}} = \frac{1}{1 + \exp\left[\frac{Z_1 Z_2 - \zeta}{\tau}\right]}, \quad (14)$$

where  $\zeta = 1760$  and  $\tau = 45$ . This expression is intended only to represent  $P_{\text{CN}}$  for cold fusion reactions with  $^{208}\text{Pb}$  or  $^{209}\text{Bi}$ . As seen in Fig. 7, this expression overestimates the values of  $P_{\text{CN}}$  for hot fusion reactions.

The “fusion by diffusion” model [5] includes a formalism for calculating  $P_{\text{CN}}$  that should be applicable to hot fusion reactions. The predictions of that formalism are also shown in Fig. 7. This model gives estimates of  $P_{\text{CN}}$  that are lower than the measured values but which generally describe the dependence of  $P_{\text{CN}}$  upon fissility.

Also included in Fig. 7 is a simple empirical representation of the data (as a dotted line); i.e., for  $x_{\text{eff}} \leq 0.58$ ,  $P_{\text{CN}} = 1$ . For  $x_{\text{eff}} \geq 0.58$ ,  $P_{\text{CN}} = \exp[-26.8(x_{\text{eff}} - 0.58)]$ .

Siwek-Wilczynska *et al.* [46] have proposed a parametrization of  $P_{\text{CN}}$  in the form of an equation

$$\log_{10}(P_{\text{CN}}) = -(z/a)^k, \quad (15)$$

where  $a \sim 145$  and  $k = 3.0$ . The variable  $z$  is given as

$$z = \frac{Z_1 Z_2}{(A_1^{1/3} + A_2^{1/3})}. \quad (16)$$

While this function is intended to describe situations where  $E^*$  is about 10 MeV above the barrier, it appears do a respectable job of representing the  $P_{\text{CN}}$  values.

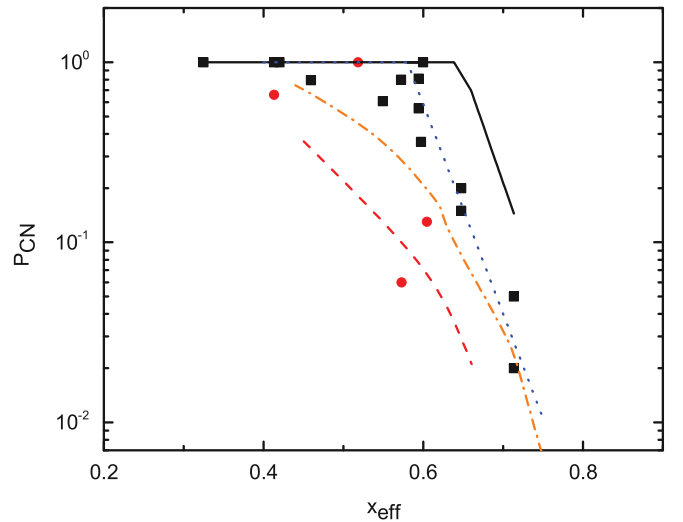


FIG. 7. (Color online) Comparison of the measurements of  $P_{\text{CN}}$  with four models for  $P_{\text{CN}}$ : solid line from [11], dashed line from [5], dot-dashed line from [46], and dotted line is a simple fit to data.

If we look carefully at the data with  $x_{\text{eff}} \sim 0.6$ , we see a variation of an order of magnitude in  $P_{\text{CN}}$  with an approximately constant value of  $x_{\text{eff}}$ . It seems clear that  $x_{\text{eff}}$  is not adequate as a single scaling variable to determine  $P_{\text{CN}}$ , as we had thought previously [51].

## V. CONCLUSION

What have we learned in this study? We have measured values of  $P_{\text{CN}}$  for four new reactions. The values of  $P_{\text{CN}}$  for the reactions of 101.2 MeV  $^{18}\text{O}$ , 147.3 MeV  $^{26}\text{Mg}$ , 170.9 MeV  $^{30}\text{Si}$ , and 195.3 MeV  $^{36}\text{S}$  with  $^{197}\text{Au}$  are 0.66, 1.00, 0.06, and 0.13, respectively. These reactions span a range of fissility used previously to compile a data set of  $P_{\text{CN}}$  values for hot fusion reactions. The new data are in rough agreement with previous measurements supporting the general dependence of  $P_{\text{CN}}$  upon fissility. Some current models for estimating  $P_{\text{CN}}$  are not adequate for quantitatively specifying  $P_{\text{CN}}$ . The effective fissility,  $x_{\text{eff}}$ , is a rough scaling variable for  $P_{\text{CN}}$ , but systems with similar  $x_{\text{eff}}$  can have  $P_{\text{CN}}$  values differing by as much as an order of magnitude.

## ACKNOWLEDGMENTS

This work was supported in part by the Director, Office of Energy Research, Division of Nuclear Physics of the Office of High Energy and Nuclear Physics of the U.S. Department of Energy, under Grant No. DE-FG06-97ER41026 and Contract No. DE-AC02-06CH11357.

[1] R. Bock *et al.*, *Nucl. Phys. A* **388**, 334 (1982).

[2] H.-G. Clerc, J. G. Keller, C.-C. Sahm, K.-H. Schmidt, H. Schulte, and D. Vermeulen, *Nucl. Phys. A* **419**, 571 (1984).

[3] A. J. Pacheco *et al.*, *Phys. Rev. C* **45**, 2861 (1992).

[4] E. V. Prokhorova *et al.*, *Exotic Nuclei Exon 2004* (World Scientific, Singapore, 2005), pp. 325–332.

- [5] W. J. Swiatecki, K. Siwek-Wilczynska, and J. Wilczynski, *Phys. Rev. C* **71**, 014602 (2005); K. Siwek-Wilczynska (private communication).
- [6] B.-A. Bain, F.-S. Zhang, and H.-Y. Zhou, *Nucl. Phys. A* **829**, 1 (2009).
- [7] V. V. Sargsyan, G. G. Adamian, N. V. Antonenko, W. Scheid, and H. Q. Zhang, *J. Phys. Conf. Ser.* **282**, 012001 (2011).
- [8] R. Vandenbosch and J. R. Huizenga, *Nuclear Fission* (Academic, New York, 1973), p. 232.
- [9] <http://nrv.jinr.ru/nrv/>.
- [10] M. Kowal, P. Jachimowicz, and A. Sobczewski, *Phys. Rev. C* **82**, 014303 (2010).
- [11] V. I. Zagrebaev and W. Greiner, *Phys. Rev. C* **78**, 034610 (2008).
- [12] G. Giardina, A. K. Nasirov, G. Mandaglio, F. Curciarello, V. De Leo, G. Fazio, M. Manganaro, M. Romanik, and C. Sacca, *J. Phys. Conf. Ser.* **282**, 012006 (2011).
- [13] R. S. Naik *et al.*, *Phys. Rev. C* **76**, 054604 (2007).
- [14] R. K. Choudhury and R. G. Thomas, *J. Phys. Conf. Ser.* **282**, 012004 (2011).
- [15] A. Nasirov, G. Giardina, G. Mandaglio, M. Mangarano, and W. Scheid, *J. Phys. Conf. Ser.* **282**, 012010 (2011).
- [16] J. P. Blocki *et al.*, *Nucl. Phys. A* **459**, 145 (1986).
- [17] P. Armbruster, *Annu. Rev. Nucl. Part. Sci.* **50**, 411 (2000).
- [18] W. J. Swiatecki, *Phys. Scr.* **24**, 113 (1981).
- [19] S. Bjornholm and W. J. Swiatecki, *Nucl. Phys. A* **391**, 471 (1982).
- [20] J. Toke *et al.*, *Nucl. Phys. A* **440**, 327 (1985).
- [21] W. Q. Shen *et al.*, *Phys. Rev. C* **36**, 115 (1987).
- [22] A. Saxena, A. Chatterjee, R. K. Choudhury, S. S. Kapoor, and D. M. Nadkarni, *Phys. Rev. C* **49**, 932 (1994).
- [23] L. M. Pant, A. Saxena, R. K. Choudhury, and D. M. Nadkarni, *Phys. Rev. C* **54**, 2037 (1996).
- [24] A. C. Berriman, D. J. Hinde, R. D. Butt, M. Dasgupta, C. P. Morton, A. Mukherjee, and J. O. Newton, *AIP Conf. Proc.* **610**, 608 (2002).
- [25] R. Sagaidak *et al.*, *AIP Conf. Proc.* **853**, 114 (2006).
- [26] T. K. Ghosh *et al.*, *Phys. Rev. C* **79**, 054607 (2009).
- [27] R. G. Thomas *et al.*, *Phys. Rev. C* **77**, 034610 (2008).
- [28] E. Prasad *et al.*, *Phys. Rev. C* **81**, 054608 (2010).
- [29] R. Rafiei, R. G. Thomas, D. J. Hinde, M. Dasgupta, C. R. Morton, L. R. Gasques, M. L. Brown, and M. D. Rodriguez, *Phys. Rev. C* **77**, 024606 (2008).
- [30] H. Q. Zhang, C. L. Zhang, C. J. Lin, A. K. Nasirov, G. Mandaglio, M. Manganaro, and G. Giardina, *J. Phys. Conf. Ser.* **282**, 012013 (2011).
- [31] G. N. Knyazheva *et al.*, *Phys. Rev. C* **75**, 064602 (2007).
- [32] S. Appannababu *et al.*, *Phys. Rev. C* **80**, 024603 (2009).
- [33] M. G. Itkis, A. A. Bogachev, E. V. Chernysheva, I. M. Itkis, G. N. Knyazheva, and E. M. Kozulin, *AIP Conf. Proc.* **1238**, 52 (2010).
- [34] B. B. Back, *Phys. Rev. C* **31**, 2104 (1985).
- [35] B. B. Back *et al.*, *Phys. Rev. C* **53**, 1734 (1996).
- [36] D. J. Hinde, R. du Rietz, M. Dasgupta, R. G. Thomas, and L. R. Gasques, *Phys. Rev. Lett.* **101**, 092701 (2008).
- [37] E. M. Kozulin, F. Gonnemann, M. G. Itkis, G. N. Knyazheva, L. Krupa, Y. T. Oganessian, and V. I. Zagrebaev, *AIP Conf. Proc.* **1175**, 138 (2009).
- [38] D. J. Hinde, R. du Rietz, R. G. Thomas, R. Rafiei, M. Dasgupta, and A. Diaz-Torres, *AIP Conf. Proc.* **1098**, 281 (2009).
- [39] V. I. Zagrebaev, *Phys. Rev. C* **64**, 034606 (2001).
- [40] V. I. Zagrebaev and W. Greiner, *J. Phys. G* **34**, 1 (2007).
- [41] Z-Q. Feng, G-M. Jin, and J-Q. Li, *Nucl. Phys. A* **836**, 82 (2010).
- [42] A. K. Nasirov, G. Giardina, A. I. Muminov, W. Scheid, and U. T. Yakhshiev, *Acta Phys. Hung. A* **19**, 109 (2004).
- [43] G. G. Adamian, N. V. Antonenko, and W. Scheid, *Nucl. Phys. A* **678**, 24 (2000).
- [44] J. Blocki, L. Shvedov, and J. Wilczynski, *Int. J. Mod. Phys. E* **15**, 426 (2006).
- [45] K. Siwek-Wilczynska, I. Skwira-Chalot, and J. Wilczynski, *Int. J. Mod. Phys. E* **16**, 483 (2007).
- [46] K. Siwek-Wilczynska, A. Borowiec, I. Skwira-Chalot, and J. Wilczynski, *Int. J. Mod. Phys. E* **17**, 12 (2008).
- [47] N. Wang and M. Liu, *Nucl. Phys. A* **834**, 212c (2010).
- [48] D. J. Hinde, C. R. Morton, M. Dasgupta, J. R. Leigh, J. C. Mein, and H. Timmers, *Nucl. Phys. A* **592**, 271 (1995).
- [49] R. du Rietz, D. J. Hinde, M. Dasgupta, R. G. Thomas, L. R. Gasques, M. Evers, N. Lobanov, and A. Wakhle, *Phys. Rev. Lett.* **106**, 052701 (2011).
- [50] D. J. Hinde, R. du Rietz, and M. Dasgupta, *EPJ Web Conf.* **17**, 04001 (2011).
- [51] P. Armbruster, *Rep. Prog. Phys.* **62**, 465 (1999).
- [52] C. Simenel, A. Wakhle, B. Avez, D. J. Hinde, R. du Rietz, M. Dasgupta, M. Evers, C. J. Lin, and D. H. Luong, *EPJ Web Conf.* **38**, 09001 (2012).
- [53] L. Corradi *et al.*, *Phys. Rev. C* **71**, 014609 (2005).
- [54] B. B. Back *et al.*, *Phys. Rev. C* **32**, 195 (1985).
- [55] V. E. Viola, Jr., T. D. Thomas, and G. T. Seaborg, *Phys. Rev.* **129**, 2710 (1963).
- [56] K. Shima, T. Ishihara, and T. Mizumo, *Nucl. Instrum. Methods* **200**, 605 (1982).
- [57] J. F. Ziegler, *Nucl. Instrum. Methods Phys. Res., Sect. B* **219**, 1027 (2004).
- [58] H. W. Schmitt, W. E. Kiker, and C. W. Williams, *Phys. Rev.* **137**, B837 (1965).
- [59] W. Reisdorf, *Z. Phys. A* **300**, 227 (1981); W. Reisdorf and M. Schädel, *ibid.* **343**, 47 (1992).
- [60] W. Loveland, *J. Phys. Conf. Ser.* **420**, 012004 (2013).
- [61] V. I. Zagrebaev, Y. T. Oganessian, M. G. Itkis, and W. Greiner, *Phys. Rev. C* **73**, 031602(R) (2006).
- [62] J. G. Keller *et al.*, *Phys. Rev. C* **36**, 1364 (1987).
- [63] S. Cohen, F. Plasil, and W. J. Swiatecki, *Ann. Phys. (N.Y.)* **82**, 557 (1974).
- [64] A. J. Sierk, *Phys. Rev. C* **33**, 2039 (1986).
- [65] M. B. Tsang *et al.*, *Phys. Rev. C* **28**, 747 (1983).
- [66] J. R. Huizenga, A. N. Behkami, and L. G. Moretto, *Phys. Rev.* **177**, 1826 (1969).
- [67] L. Lyons, *A Practical Guide to Data Analysis for Physical Science Students* (Cambridge University Press, Cambridge, 1991).
- [68] I. M. Itkis *et al.*, *Phys. Rev. C* **83**, 064613 (2011).
- [69] E. M. Kozulin *et al.*, *Phys. Lett. B* **686**, 227 (2010).